Journal of Pain Research

Dovepress
Taylor & Francis Group

Open Access Full Text Article

ORIGINAL RESEARCH

Transcranial Direct Current Stimulation Targeting the Primary Motor Cortex Suppresses Activity in the Ventrolateral Periaqueductal Gray and Alleviates Chronic Pain in a Rat Model of Knee Osteoarthritis

Yifan Xu[1], Chenglei Fan[2], Junqiang Xue[1], Chengfei Gao[1], Yu Zhou[3], Tieshan Li[1]

[1]Department of Rehabilitation Medicine, The Affiliated Hospital of Qingdao University, Qingdao, Shandong Province, People's Republic of China; [2]School of Rehabilitation Sciences and Engineering, University of Health and Rehabilitation Sciences, Qingdao, Shandong Province, People's Republic of China; [3]Department of Life Sciences and Health, University of Health and Rehabilitation Sciences, Qingdao, Shandong Province, People's Republic of China

Correspondence: Tieshan Li; Yu Zhou, Email tieshanli@qdu.edu.cn; yuzhou@uhrs.edu.cn

Journal of Pain Research downloaded from https://www.dovepress.com/
For personal use only.

Purpose: Transcranial direct current stimulation (tDCS) shows promise for chronic pain treatment; however, its efficacy and mechanisms in knee osteoarthritis (KOA)-associated pain remain unclear. This study aimed to evaluate the analgesic effects of primary motor cortex (M1)-targeted tDCS in a rat model of KOA and to investigate the underlying mechanisms.

Methods: A chronic KOA model was established via unilateral intra-articular monoiodoacetate (MIA) injection. Mechanical allodynia and thermal hyperalgesia were assessed using von Frey filaments and a hot plate test. Neuronal activation and microglial responses in the ventrolateral periaqueductal gray (vlPAG) were evaluated by immunohistochemistry, and inflammatory cytokines were quantified using qPCR. The effects of M1-targeted tDCS on vlPAGactivity, microglial activation, and pain behaviors were examined. Minocycline was administered into the vlPAG to inhibit microglial. CTB-555 retrograde tracing was used to map M1-vlPAG connectivity.

Results: MIA induced persistent pain hypersensitivity, accompanied by increased neuronal activity, microglial activation, and elevated pro-inflammatory cytokines in the contralateral vlPAG. Local administration of minocycline suppressed both microglial and neuronal activation and alleviated pain behaviors. M1-targeted tDCS significantly reduced pain hypersensitivity, suppressed vlPAG neuronal activity and microglial activation, and downregulated inflammatory cytokines expression.

Conclusion: KOA-associated chronic pain is linked to increased neuronal activity and neuroinflammation in the vIPAG. M1-targeted tDCS alleviates pain, likely by suppressing vIPAG activity and microglial-mediated inflammation via the M1-vlPAG pathway. However, given differences between the MIA model and human osteoarthritis, caution is required in clinical translation.

Keywords: transcranial direct current stimulation, knee osteoarthritis, chronic pain, microglial, neuroinflammation, M1-vlPAG pathway

Introduction

Knee osteoarthritis (KOA) is a degenerative joint disorder characterized by progressive articular cartilage degradation and chronic pain.[1,2] Current management strategies for KOA include pharmacological treatment, patient education, weight management, and exercise-based physiotherapy.[3] In particular, exercise therapy is widely recommended as a first-line intervention in major clinical guidelines due to its beneficial effects on pain, physical function, and quality of life.[4] However, despite these guideline-recommended approaches, a substantial proportion of patients continue to experience persistent pain and functional limitations. Moreover, pharmacological treatments often provide limited efficacy and may be associated with significant adverse effects.[5] Notably, even after total joint arthroplasty, up to 20% of patients report persistent chronic pain,[6] suggesting that KOA-related pain is not solely attributable to peripheral joint degeneration but is also closely linked to central sensitization mechanisms.[7,8] The frequent discrepancy between structural imaging findings and subjective pain perception further underscores the critical contribution of central mechanisms to KOA-associated chronic pain.[9] Therefore, it is necessary to explore novel adjunctive, non-pharmacological therapeutic strategies.

https://doi.org/10.2147/JPR.S595212
Received: 30 January 2026
Accepted: 25 April 2026
Published: 6 May 2026

© 2026 Xu et al. This work is published and licensed by Dove Medical Press Limited. The full terms of this license are available at https://www.dovepress.com/terms.php and incorporate the Creative Commons Attribution – Non Commercial (unported, v4.0) License (http://creativecommons.org/licenses/by-nc/4.0/). By accessing the work you hereby accept the Terms. Non-commercial uses of the work are permitted without any further permission from Dove Medical Press Limited, provided the work is properly attributed. For permission for commercial use of this work, please see paragraphs 4.2 and 5 of our Terms (https://www.dovepress.com/terms.php).

Central sensitization is a key neuropathological mechanism underlying the initiation, development, and maintenance of chronic pain.[10,11] The ventrolateral periaqueductal gray (vlPAG) is a key brain region involved in descending pain modulation, functioning through the PAG-rostral ventromedial medulla (RVM)-spinal dorsal horn (SDH) pathway.[12,13] Neurons within the vlPAG exhibit functional heterogeneity: activation of GABAergic neurons can induce hyperalgesia,[14] whereas activation of glutamatergic or dopaminergic neurons promotes analgesia.[15] In addition, BDNF-expressing neurons within the vlPAG project to the RVM and contribute to both opioid-induced analgesia and inflammation-related hyperalgesia, highlighting the complex and bidirectional regulation of pain within this region.[16,17] Given its central role in descending pain control, alterations in neuronal activity and neuroinflammatory processes within the vlPAG may critically contribute to central sensitization in chronic pain. However, whether the vlPAG is directly involved in the pathogenesis of KOA-associated chronic pain, and whether its modulation contributes to analgesia, remains unclear. Addressing these questions is of particular translational importance, as dysfunction of descending pain modulation is increasingly recognized as a major contributor to persistent pain in clinical populations.[18–20]

Microglial, the resident immune cells of the central nervous system, play a central role in the development and maintenance of chronic pain.[21] Through dynamic interactions with neurons, microglial regulate synaptic transmission and plasticity.[22] Upon injury or inflammatory stimulation, microglial become activated, exhibiting morphological changes and releasing pro-inflammatory mediators such as IL-1β, TNF-α, and IL-6.[23] These cytokines promote the expression and function of neuronal NMDA receptors, enhance neuronal excitability, disrupt the excitatory/inhibitory balance, and thereby contribute to central sensitization.[24] Conversely, neuronal signals such as CX3CL1 and ATP further activate microglial through receptors including CX3CR1 and P2X4/P2X7, forming a feed-forward loop that exacerbates neuroinflammation and pain signaling.[25,26] In osteoarthritis models, inhibiting microglial activation in the spinal dorsal horn effectively alleviates pain hypersensitivity.[27,28] Similarly, microglial activation within the vlPAG has been shown to enhance descending facilitation pathways and amplifying pain signals.[29] However, whether vlPAG microglial contribute to KOA-associated chronic pain remains unclear. Supraspinal neuroinflammation may help explain why osteoarthritis pain often persists independent of peripheral joint pathology, highlighting a promising central target for therapeutic intervention.

Transcranial direct current stimulation (tDCS) is a safe, non-invasive neuromodulation technique that applies a weak direct current (typically 0.5–1 mA) to the scalp to modulate cortical excitability.[30] It has been widely investigated as an adjunctive treatment for chronic pain and various neurological and neuropsychiatric disorders due to its low cost, portability, and favorable safety profile.[31] The analgesic effects of tDCS are thought to involve stimulation of the primary motor cortex (M1), which in turn engages descending pain inhibitorypathways.[32] Previous studies have shown that M1-targeted tDCS suppresses microglial activation in the PAG and relieves chronic neuropathic pain following spinal cord injury.[33] Our previous work further demonstrated that M1-targeted tDCS alleviates chronic pain in KOA rats by modulating the BDNF/TrkB signaling pathway and GluN2B expression within the PAG-RVM-SDH axis.[34,35] Although tDCS is applied at the cortical level,[36] accumulating evidence suggests that its effects extend to subcortical structures, including the thalamus and PAG, via descending modulatory circuits.[36,37] However, direct evidence demonstrating whether and how M1-targeted tDCS modulates neuronal activity and microglial-mediated neuroinflammation specifically within the vlPAG remains lacking. In addition, the exclusive use of male animals in preclinical studies limits the generalizability of findings, given known sex differences in pain processing. Although tDCS shows promise in clinical settings, the current level of evidence for KOA remains moderate, and it is not yet universally recommended in clinical guidelines.[38,39] Therefore, further mechanistic studies are needed to elucidate its central neurobiological effects.

In the present study, we investigated the role of the vlPAG in chronic pain using a monoiodoacetate (MIA)-induced rat model of KOA. We further aimed to elucidate the supraspinal mechanisms by which M1-targeted tDCS exerts its analgesic effects, with a particular focus on neuronal activity and microglial-mediated neuroinflammation within the vlPAG.

Material and Methods

Animals and Ethics Statement

A total of 64 male Sprague-Dawley (SD) rats (200±20 g) were used in this study. Male animals were exclusively selected to maintain consistency and minimize biological variability associated with sex-dependent hormonal fluctuations during

this initial mechanistic investigation. All animals were obtained from Jinan Pengyue Experimental Animal Breeding Co., Ltd. Rats were housed 5 per cage under controlled environmental conditions (temperature 22±2°C, 12 h light/dark cycle) with ad libitum access to food and water. Animals were allowed to acclimatize to the laboratory environment for at least 7 days prior to any experimental procedures. All experimental protocols were approved by the Animal Ethics and Welfare Committee of Qingdao University (Approval No.: 20240710SD6420240821092) and conducted in accordance with relevant guidelines.

Animal Model

Monoiodoacetate (MIA) induces cartilage degeneration by disrupting chondrocyte metabolism and reliably reproduces the histopathological changes and chronic pain associated with KOA.[40] On day 0, rats under isoflurane anesthesia received an intra-articular injection of 60 μL of MIA solution (80 mg/mL; Sigma, USA) into the left knee joint cavity via the infrapatellar ligament.[41] The sham group received an equal volume of 0.9% saline.

Experimental Design

This study consisted of two main parts:

Role of vlPAG in KOA-Associated Chronic Pain

Rats were randomly assigned to a sham-operated group (Sham) and an MIA group (n=5 per group). Pain-related behaviors were assessed at baseline (day −1) and on days 1, 3, 7, 14, and 23 post-injection. Based on behavioral outcomes and the established progression of the MIA model, day 14 was defined as the chronic pain stage, at which point pain hypersensitivity was stable Therefore, animals were euthanized on day 14, and brain tissues were collected for immunohistochemical analyses.

A separate cohort of MIA-treated rats were then randomly assigned into a MIA+NS control group and a MIA +minocycline intervention group (n=4 per group). All animals underwent stereotaxic cannulation targeting the vlPAG 7 days prior to MIA injection. Starting from the day of modeling, animals received daily intra-vlPAG microinjections of minocycline or saline for 14 consecutive days. Behavioral assessments were conducted on day −1 and on days 1, 3, 7, and 14 after modeling. Brain tissues were collected on day 14 to evaluate the effects of microglial inhibition during both the development and maintenance phases of chronic pain.

Mechanisms of M1-Targeted tDCS

To examine anatomical connectivity, CTB-555 was injected into the vlPAG, and brain tissues were collected 2 weeks later to allow sufficient retrograde transport and stable neuronal labeling.[42] Immunofluorescence staining was performed to identify direct projections from M1 to the vlPAG.

In a separate cohort, MIA-treated rats were randomly assigned to MIA+tDCS or MIA+StDCS (shamstimulation) groups (n=5 per group). tDCS treatment was initiated on day 14 post-MIA injection, corresponding to the established chronic pain phase, in order to evaluate therapeutic rather than preventive effects. Animals received daily stimulation for 8 consecutive days. Behavioral tests were conducted 1 day and 7 days after treatment to assess both short-term and sustained effects. Brain tissues were collected 7 days after tDCS treatment to evaluate lasting neurobiological changes.

Sample sizes were determined based on our previous work, relevant published literature using comparable MIA-induced KOA models,[34,35,43] and ethical considerations to minimize animal use in accordance with the 3Rs principle. Given that certain experiments were exploratory in nature, relatively small group sizes were employed. To ensure statistical rigor, appropriate statistical analyses were applied, and post hoc power analyses were conducted for key outcomes (Supplementary Table 1).

Randomization and Blinding

Animals were randomly assigned to experimental groups using a computer-generated randomization sequence. Each animal was assigned a coded identification number, and group allocation was concealed from investigators involved in behavioral testing, data acquisition, and analysis whenever feasible. Blinding was not possible during certain procedures

(eg., model induction, stereotaxic surgery, or tDCS administration) due to their technical nature. However, these procedures were performed by operators not involved in outcome assessment. Behavioral testing, histological analysis, and data quantification were conducted by investigators blinded to group allocations. All tissue samples and images were coded prior to analysis. Unblinding was performed only after completion of all primary data analyses.

Pain Behavioral Assessment

All behavioral tests were conducted under controlled environmental conditions (22–25°C) in a quiet room. To minimize environmental stress, noise and unnecessary disturbances were reduced as much as possible during testing. Mechanical sensitivity was assessed prior to thermal testing with a 2-hour interval to minimize potential interference. Animals were acclimated to the testing environment for at least 30 min prior to each session. All tests were conducted at consistent times of day. Behavioral assessments were performed on the ipsilateral hind paw, corresponding to the MIA-injected joint, to specifically evaluate localized pain hypersensitivity The contralateral hind paw was not analyzed, as the primary objective was to assess unilateral pain responses. Animals were excluded from behavioral analysis if they failed to adapt to the testing environment, exhibited abnormal baseline nociceptive thresholds, showed poor general condition, had unsuccessful model induction or tissue processing failure. A total of 8 animals were excluded All exclusion criteria were predefined and applied prior to data analysis, independent of experimental outcomes. All tests and measurements were performed by the same experimenter under standardized conditions, and all procedures were carried out with the experimenter blinded to group assignments.

Mechanical Allodynia

Mechanical nociceptive sensitivity was assessed by measuring the 50% paw withdrawal threshold (PWT) using von Frey filaments and "Dixon's up-down method".[44] For mechanical sensitivity testing, von Frey filaments were used according to the manufacturer's instructions. The integrity of the filaments was checked before each testing session to ensure consistent bending force. Rats were acclimated for 30 minutes in transparent enclosures placed on an elevated wire mesh floor. PWT was determined using the up-down method by applying a series of von Frey filaments (0.16g to 26.0g) to the mid-plantar surface of the left hind paw. Testing always commenced with the 2.0 g filament, and each filament was applied 5 times with an inter-stimulus interval of 7s. A rapid withdrawal was recorded as a positive response. This procedure was repeated three times per animal with ≥ 30 min inter-test intervals and the average PWT was calculated. The 50% threshold (in grams) was derived using the formula: 50% threshold = $(10^{[Xf + K\delta]})/10{,}000$.

Thermal Hyperalgesia

Thermal pain sensitivity was assessed using a hot plate maintained at 55 ± 0.2°C. Before use, the apparatus was preheated, and the surface temperature was confirmed before each test according to the manufacturer's instructions. The equipment was regularly calibrated to ensure measurement accuracy and consistency. The paw withdrawal latency (PWL), defined as the time to hind paw licking/flicking, jumping, or vocalization, was recorded.[45] Each rat underwent three trials, with an inter-trial interval of ≥30 min, and the mean latency was calculated. A cut-off time of 30s was used to prevent tissue damage.

tDCS Treatment

Rats received tDCS (0.5 mA, 20 min/day) for 8 consecutive days beginning on day 14 post-MIA injection.[34] During stimulation, animals were briefly anesthetized with isoflurane (5% induction;1.5–2% maintenance) to ensure stable electrode placement and minimize movement. To reduce potential confounding effects of repeated anesthesia, all groups underwent identical anesthetic procedures with standardized duration and depth. The duration of anesthesia was limited to the minimum required to complete electrode placement and stimulation (approximately 20 min per session). The depth of anesthesia was kept at a light level, sufficient to prevent struggling and allow stable electrode contact, while spontaneous respiration was maintained throughout the procedure. The depth of anesthesia was monitored throughout the procedure by assessing respiratory pattern and the absence of response to a paw pinch/toe pinch, and additional anesthetic was administered only when necessary. Two rubber surface electrodes (1.5 cm^2 each) coated with conductive gel were placed on the scalp and

secured with adhesive tape to ensure stable electrode-skin contact throughout the stimulation period. The anode was positioned over the right primary motor cortex, and the cathode was placed over the contralateral supraorbital region. Current was gradually ramped up and down over 10–30s to ensure stable delivery. A constant current of 0.5 mA was delivered, corresponding to a current density of 0.33 mA/cm^2, without causing brain lesions.[46,47] Although real-time impedance monitoring was not available, variability was minimized by standardizing electrode placement, skin preparation, and stimulation parameters. All procedures were performed by the same trained experimenter. Sham stimulation involved identical procedures, with current delivered only during the initial 30s. After stimulation, animals were returned to their home cages and allowed to fully recover before any subsequent behavioral assessment.

Stereotaxic Surgery

Rats were anesthetized with isoflurane and placed in a stereotaxic frame. vlPAG coordinates relative to bregma (AP: −7.60 mm, ML: +0.65 mm, DV: −5.90 mm) were determined with reference to the Paxinos & Watson brain atlas and previous studies.[29,48] A total of 250 nL of the retrograde tracer CTB-555 (1 μg/μL, BrainVTA) was microinjected at 0.03μL/min, and the needle was left in place for 10 min to prevent reflux. Animals were allowed to recover fully before subsequent procedures. During this period, their overall condition was continuously monitored, including activity, food intake, and wound healing, to ensure physiological stability. Although stereotaxic surgery and anesthesia may induce nonspecific physiological effects, the purpose of this experiment was to determine the anatomical projection from M1 to the vlPAG rather than to evaluate stress or inflammation-related responses. All surgeries were performed under standardized conditions to minimize variability and potential confounding effects.

Local Drug Infusion in the vlPAG

Minocycline was administered via intra-vlPAG microinjection using a stereotaxically implanted guide cannula (OD 0.56 mm; ID 0.38 mm; RWD). The optimal coordinates (AP: −7.60 mm, ML: +0.65 mm, DV: −5.90 mm relative to bregma) were prevalidated in a separate cohort prior to the main experiments by infusing 500 nL of Evans Blue dye. Histological analysis confirmed that the infusion was confined to the vlPAG. During surgery, the cannula was firmly secured to the skull using stainless-steel screws and dental cement. Following cannula implantation, animals were allowed a 7-day postoperative recovery period prior to behavioral testing. During this period, their general physiological condition, including spontaneous activity, food intake, and wound healing, was closely monitored to ensure stability. For pharmacological intervention, minocycline (Selleckchem, USA) was dissolved in normal saline to a final concentration of 15 μg/μL.[49] Drug microinjections were performed 20 minutes prior to behavioral testing in awake, freely moving animals to avoid anesthesia-related confounding effects. The drug was delivered using a microinjection pump (Stoelting, USA) connected to a Hamilton syringe via BC-22 tubing. An injection cannula (OD 0.36 mm; ID 0.20 mm; RWD), extending 1 mm beyond the tip of the guide cannula, was inserted. Each rat received a unilateral infusion of 500 nL minocycline or normal saline into the right vlPAG at a slow, controlled rate to minimize local tissue damage. After infusion, the injection cannula was left in place for an additional 5 min before gentle withdrawal to prevent reflux along the needle tract. To minimize procedural variability, all surgicalprocedures, handling, and microinjections were performed by the same trained experimenter across all groups.

Immunofluorescence Staining

Under deep anesthesia, rats were transcardially perfused with 0.9% saline followed by 4% paraformaldehyde. After postfixation, brain were cryoprotected in 30% sucrose and coronally sectioned at 40μm. The vlPAG was identified according to the Paxinos and Watson atlas, and sections spanning approximately AP −7.50 mm to −8.70 mm were collected using the cerebral aqueduct as a landmark. Free-floating sections were blocked with 5% normal goat serum containing 0.3% Triton X-100 for 1.5 h, followed by incubation with primary antibodies at 4°C overnight. The next day, sections were incubated with secondary antibodies at room temperature for 1.5 h, and nuclei were counterstained with DAPI before mounting. Primary antibodies included rabbit anti-c-Fos (1:500, Cell Signaling Technology) and rabbit anti-Iba-1 (1:1000, Cell Signaling Technology). The secondary antibody was Alexa Fluor 488-conjugated goat anti-rabbit IgG (1:1000, ABclonal). Images were acquired using an Olympus VS120 virtual slide microscope. All images within the

same experiment were captured using identical acquisition settings to ensure comparability across groups. Image stitching and processing were performed using OLYMPUS OlyVIA software (version 3.3). For figure presentation, brightness and contrast were adjusted uniformly across entire images and applied consistently across all groups. No selective enhancement, deletion, or manipulation of specific image features was performed. Subsequent image processing and quantitative analysis were conducted using Fiji/ImageJ (version 1.54f). Morphological analyses were performed using the Analyze Skeleton and Sholl analysis plugins. For each animal, three representative vlPAG sections were selected, and 3–4 regions of interest (ROIs) per section were quantified.

Quantitative Real-Time PCR (qRT-PCR)

Total RNA was extracted from the vlPAG using the PureLink RNA Mini Kit (Thermo Fisher Scientific). After quantification with NanoDrop, RNA was reverse-transcribed into cDNA using SuperScript III Reverse Transcriptase (Invitrogen). Quantitative PCR was performed using the SYBR Green method (Qiagen) under the following cycling conditions: initial denaturation at 95°C for 5 min, followed by 40 cycles of 95°Cfor 5s, 60°C for 30s, and 72°C for 30s. Relative expression levels of target genes were calculated using the $2^{-\Delta\Delta CT}$ method, with Gapdh as the endogenous control.

The sequences of the PCR primers (Sangon Biotech) were:

Gapdh: F: 5'-TTGTGAAGCTCATTTCCTGGTA-3', R: 5'-GGCCTCTCTCTTGCTCTCAGTA-3'

IL-6: F: 5'-AGTTGCCTTCTTGGGACTGA-3', R: 5'-ACTGGTCTGTTGTGGGTGGT-3'

IL-1β: F: 5'-GCTGTGGCAGCTACCTATGTCTTG-3', R: 5'-AGGTCGTCATCATCCCACGAG-3'

Tnf-α: F: 5'-GGTTCCGTCCCTCTCATACA-3', R: 5'-AGACACCGCCTGGAGTTCT-3'

IL-4: F: 5'-CAACAAGGAACACCACGGAGAAC-3', R: 5'-CTTCAAGCACGGAGGTACATCAC-3

IL-10: F: 5'-TGGAGTGAAGACCAGCAAAG-3', R: 5'-GGCAACCCAAGTAACCCTTA-3'

c-Fos: F: 5'-CGTCTTCCTTTGTCTTCACCTACC-3', R: 5'-GTTGCTGCTGCTGCCCTTTC-3'

All reactions were performed in triplicate.

Statistical Analysis

Data are presented as mean ± standard deviation (Mean ± SD). Statistical analyses were performed using GraphPad Prism (version 10.1.2). Normality and homogeneity of variance were assessed prior to analysis. Behavioral data were analyzed using two-way repeated-measures ANOVA followed by Sidak's post hoc tests. Other comparisons were conducted used unpaired two-tailed Student's *t*-test or appropriate nonparametric tests when assumptions were not met. To improve transparency, individual data points are presented in all figures. Post hoc power analyses were conducted for experiments with small sample sizes using G*Power 3.1.9.7 to strengthen the statistical rigor, and these results are reported in Supplementary Table 1. A P value < 0.05 was considered statistically significant.

Results

MIA Injection Induces vlPAG Activation in KOA Model Rats

Rats with comparable baseline pain thresholds were selected for model establishment. Following intra-articular MIA injection, nociceptive behaviors were evaluated at multiple time points (Figure 1A). Compared with the sham control group, the MIA group exhibited a significant decrease in PWT and PWL beginning on day 1 post-modeling, reaching the lowest levels on day 14. This pain hypersensitivity persisted until day 23, whereas no significant changes were observed in the sham control group (Figure 1B and C; Two-way repeated measure ANOVA and Sidak's multiple comparisons test, Sham vs. MIA, PWT: d1-d23, $P < 0.0001$. PWL: d1-d23, $P < 0.001$ to $P < 0.0001$). These results indicate that the MIA model successfully induces stable chronic pain hypersensitivity. Based on this, day 14 after MIA injection was defined as the time point for successful establishment of KOA-related chronic pain.

To further explore central mechanisms underlying KOA pain, neuronal activation across PAG subregions was examined. Immunohistochemistry revealed a significant increase in c-Fos-positive neurons in the PAG of MIA-model rats, with the most marked activation observed in the vlPAG (Figure 1D–G; unpaired *t*-test, Sham vs. MIA, dlPAG: $P < 0.05$; lPAG: $P < 0.01$; vlPAG: $P < 0.0001$). Taken together, these findings indicate that MIA-induced KOA not only

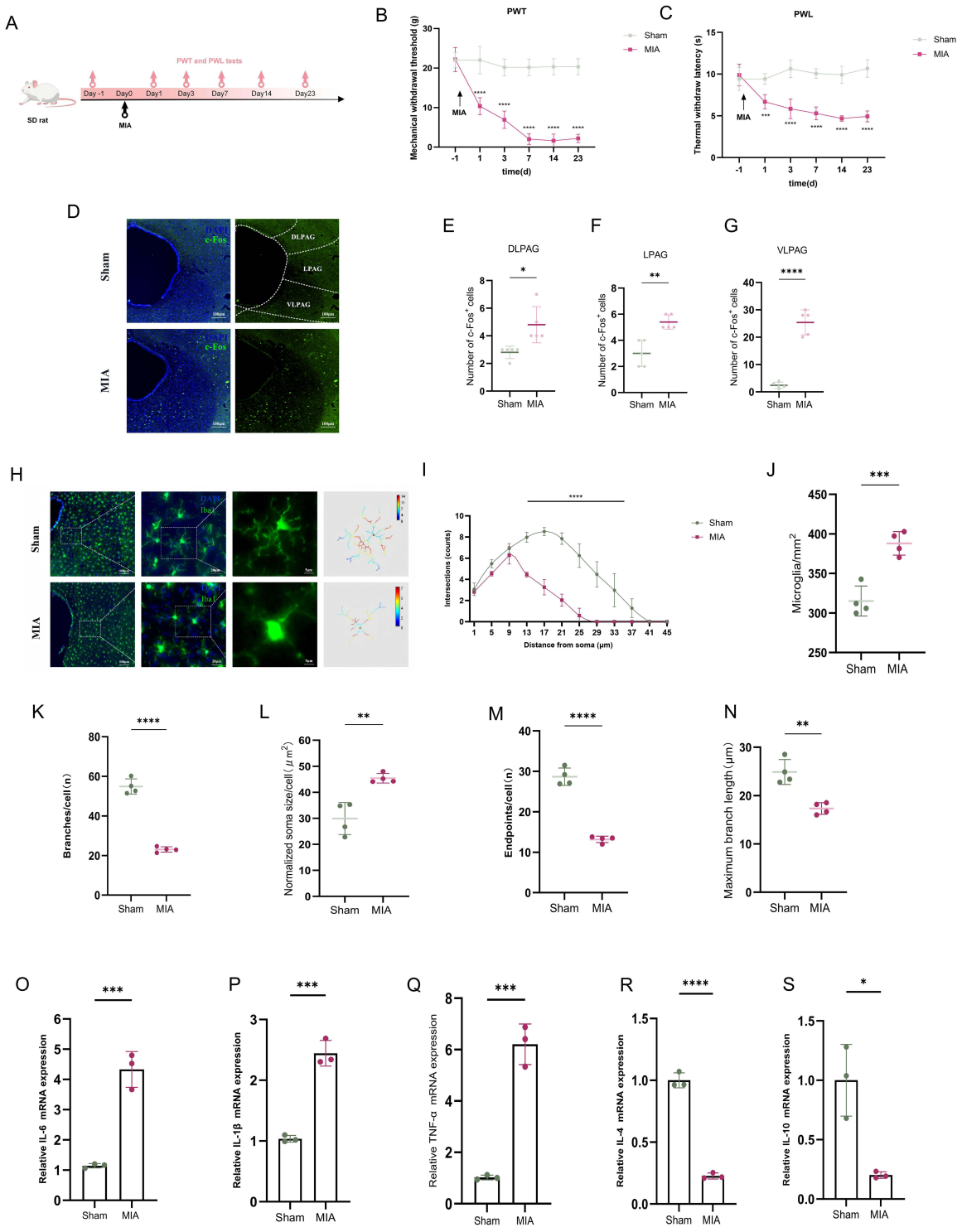

Figure 1 MIA-induced hyperalgesia and increased activity of the vlPAG in a KOA rat model. (**A**) Experimental design. (**B** and **C**) Behavioral tests. (**B**) PWT: treatment × Time F (5, 24) = 24.12, P <0.0001; time F (5, 24) = 45.90, P <0.0001; treatment F (1, 24) = 494.4, P<0.0001. (**C**) PWL: treatment × time F (5, 24) = 15.24, P <0.0001; treatment F (1, 24) = 243.1, P <0.0001; time F (5, 24) = 7.167, P <0.001. n = 6 rats per group. (**D**) Representative images showing c-Fos expression in sham and MIA-treated rats. Scale bar: 100 μm. (**E**–**G**) Quantitative analyses of c-Fos$^+$ neurons in subregions of PAG. dlPAG (**E**): t=3.244, P < 0.05; lPAG (**F**): t =4.707, P < 0.01; and vlPAG (**G**): t =10.9, P <0.0001. n = 5 rats per group. (**H**) Representative images showing Iba-1$^+$ microglial in the vlPAG and the corresponding heatmap. Scale bars: 100μm (left), 20μm (middle), 5μm (right). (**I**) Sholl analysis about intersections with concentric circles. Treatment × distance from soma F (11, 72) = 27.07, P <0.0001; treatment F (1, 72) = 399.7, P <0.0001; distance from soma F (11, 72) = 119.9, P <0.0001. n = 4 rats per group. (**J**–**N**) microglial number and morphology analysis. Microglial counts/mm^2 (**J**): t =6.035, P < 0.001; branches/cell (**K**): t =15.52, P <0.0001; soma size/cell (**L**): t =4.830, P < 0.01; terminal endpoints (**M**): t =13.52, P <0.0001; and maximum process length (**N**): t =5.308, P < 0.01. n = 4 rats per group. (**O**–**S**) RT-qPCR analyses for inflammatory factors expression in the vlPAG. IL-6 (**O**): t =9.258, P < 0.001; IL-1β (**P**): t =11.16, P < 0.001; TNF-α (**Q**): t =11.31, P < 0.001; IL-4 (**R**): t =20.46, P <0.0001; and IL-10 (**S**): t =4.566, P < 0.05. n = 3 rats per group. All data are presented as mean ± SD. *P < 0.05, **P < 0.01, ***P < 0.001, ****P < 0.0001.

https://doi.org/10.2147/JPR.S595212

produces long-lasting pain hypersensitivity but is also accompanied by pronounced neuronal activation in the vlPAG, suggesting a critical role for this region in central pain modulation.

vlPAG Microglial Exhibit Pro-Inflammatory Activation in the KOA Model Rats

To determine whether vlPAG microglial activation involves in chronic KOA pain, we analyzed microglial status in this region. Immunofluorescence staining and the Sholl analysis heatmap showed a significant increase in Iba-1 expression in vlPAG microglial of MIA-model rats compared with sham controls (Figure 1H). Sholl analysis further revealed the pro-inflammatory activation of microglial in the MIA group: reduced intersections with concentric circles (Figure 1I; Two-way repeated measure ANOVA and Sidak's multiple comparisons test, Sham vs. MIA, P <0.0001 at 13–33μm), greater counts, fewer branches, larger soma size, and shortened terminal branches and maximum branch length (Figure 1J–N; unpaired t- test, Sham vs. MIA, $P < 0.01$ to $P < 0.0001$), indicating a transition from a resting to an activated state. Our qPCR analysis revealed significant upregulation of pro-inflammatory cytokine IL-6, IL-1β, and TNF-αin the vlPAG of MIA-modeled rats (Figure 1O–Q; unpaired t test, Sham vs. MIA, $P < 0.001$), along with marked downregulation of anti-inflammatory cytokines IL-4 and IL-10 (Figure 1R and S; unpaired t-test, Sham vs. MIA, $P < 0.05$ to $P < 0.0001$). Taken together, these findings demonstrate pro-inflammatory activation of vlPAG microglial that may contribute to KOA chronic pain induced by MIA injection.

Inhibiting Microglial Activation in vlPAG Alleviates Chronic Pain Behaviors in KOA Model Rats

To confirm the involvement of vlPAG microglial in KOA pain, stereotaxic cannulation into the vlPAG was performed 7 days before MIA injection, followed by 14 days of local administration of minocycline or normal saline (NS) starting on the day of MIA injection (Figure 2A). Prior to the formal experiments, cannula placement was verified using Evans Blue dye according to stereotaxic atlas coordinates, confirming that the injection sites were accurately localized within the vlPAG (Figure 2B). Behavioral assessments showed that, compared with the MIA+NS group, the MIA+ Mino group exhibited significantly increased PWT and PWL after the first day of injection, with this analgesic effect maintained throughout the 14-day treatment period (Figure 2C and D; Two-way repeated measure ANOVA and Sidak's multiple comparisons test, MIA+NS vs. MIA+Mino, PWT: d1-d14, $P < 0.05$ to $P < 0.0001$. PWL: d1-d14, $P < 0.01$ to $P < 0.0001$). These results indicate that inhibition of vlPAG microglial activation effectively alleviates pain-related behaviors.

Immunofluorescence further revealed a significantly lower number of c-Fos-positive neurons in the vlPAG of the MIA+Mino group compared with the MIA+NS group (Figure 2E and F; unpaired t-test, MIA+NS vs. MIA+Mino in vlPAG: $P < 0.0001$), indicating reduced neuronal activation following microglial inhibition. In addition, Immunofluorescence staining and the Sholl analysis heatmap showed the MIA+Mino group displayed reduced microglial density and a resting-state morphology (Figure 2G). Sholl analysis confirmed increased intersections (Figure 2H; Two-way repeated measure ANOVA and Sidak's multiple comparisons test, MIA+NS vs. MIA+Mino, $P < 0.0001$ at 13–37μm), greater cell counts, more branches, higher numbers of terminal branches, longer maximum branch length, and smaller soma size (Figure 2I–M; unpaired t-test, MIA+NS vs. MIA+Mino, $P < 0.05$ to $P < 0.001$). In summary, our findings indicate that inflammatory activation of vlPAG microglial contributes to chronic KOA pain, whereas suppressing microglial activation reduces vlPAG neuronal activity and alleviates pain behaviors.

M1-Targeted tDCS Significantly Alleviates Pain Hypersensitivity in KOA Model Rats

To evaluate the analgesic efficacy of tDCS in the KOA model, MIA-treated rats received either M1-targeted tDCS or sham stimulation for 8 consecutive days starting on day 15 after MIA injection. PWT and PWL were measured on day 15, 22, and 29 (Figure 3A). Both PWT and PWL were significantly increased in the tDCS group, and this analgesic effect persisted until day 29 (Figure 3B and C; Two-way repeated measure ANOVA and Sidak's multiple comparisons test, MIA+tDCS vs. MIA+StDCS, PWT: $P < 0.001$ to P <0.0001, PWL: $P < 0.0001$). These findings demonstrate that M1-targeted tDCS effectively reverses MIA-induced mechanical allodynia and thermal hyperalgesia.

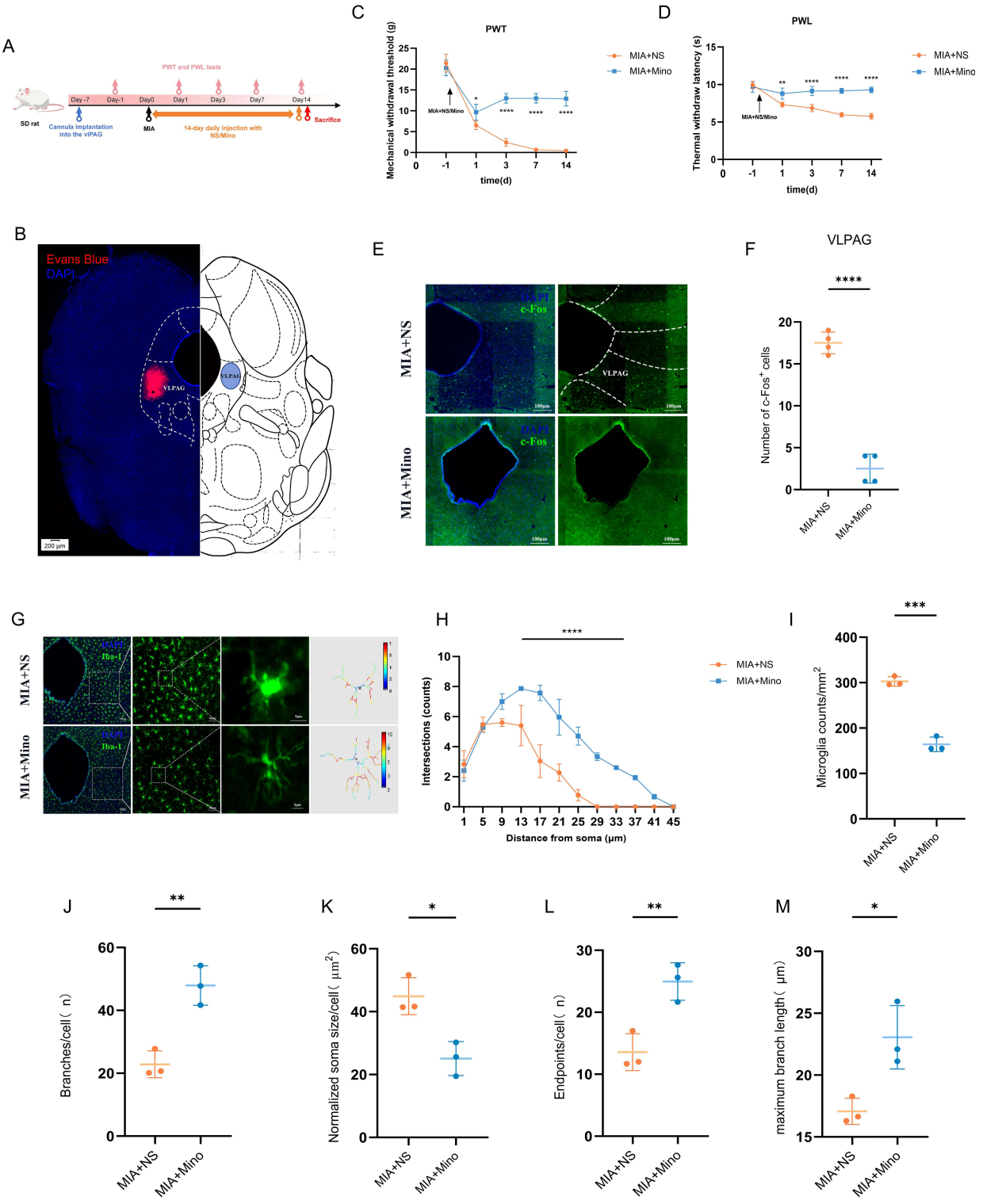

Figure 2 Minocycline administration in the vlPAG alleviates hyperalgesia and suppresses neuronal activity in KOA model rats by inhibiting microglial activation. (**A**) Experimental design. (**B**) Histological verification of the Evans Blue injection site in the vlPAG. (**C** and **D**) Behavioral tests. PWT (**C**): group × time F (4, 24) = 57.88, P <0.0001; time F (4, 24) = 227.4, P <0.0001; group F (1, 6) = 122.8, P <0.0001. PWL (**D**): group × time F (4, 24) = 24.00, P <0.0001; time F (4, 24) = 36.86, P <0.0001; group F (1, 6) = 87.09, P <0.0001. n = 4 rats per group. (**E**) Representative images showing c-Fos expression in the vlPAG. Scale bar: 100μm. (**F**) The number of c-Fos$^+$ neurons in the vlPAG: t =13.89, P <0.0001. n = 4 rats per group. (**G**) Representative images showing Iba-1$^+$ microglial in vlPAG and the corresponding heatmap. Scale bars: 100μm (left), 50μm (middle), 5μm (right). (**H**) Sholl analysis about intersections with concentric circles. Group × distance from soma F (11, 48) = 13.78, P <0.0001; group F (1, 48) = 224.0, P <0.0001; distance from soma F (11, 48) = 104.5, P <0.0001. n = 3 rats per group. (**I**–**M**) microglial number and morphology analysis. Microglial counts/mm^2 (**I**): t =12.58, P < 0.001; branches/cell (**J**): t =5.714, P < 0.01; soma size/cell (**K**): t =4.309, P < 0.05; terminal endpoints (**L**): t =4.647, P < 0.01; maximum process length (**M**): t=3.742, P < 0.05. n = 3 rats per group. All data are presented as mean ± SD. *P < 0.05, **P < 0.01, ***P < 0.001, ****P < 0.0001.

https://doi.org/10.2147/JPR.S595212

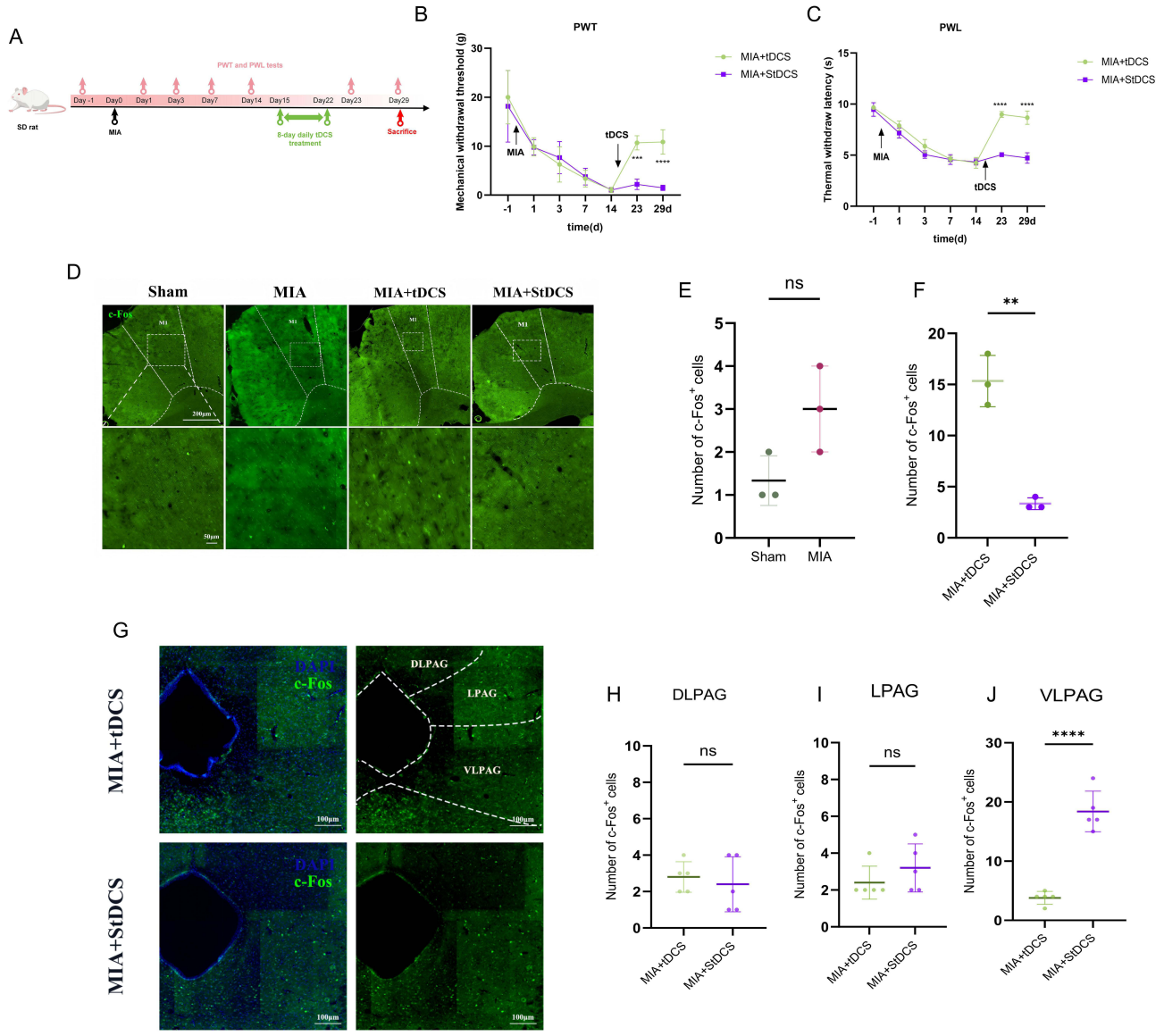

Figure 3 M1-targeted tDCS treatment alleviates pain sensitization and activates M1 meanwhile suppresses vlPAG hyperactivity in KOA model rats. (**A**) Experimental design. (**B** and **C**) Behavioral tests. PWT(**B**): group × time F (6, 56) = 5.365, P <0.001; group F (1, 56) = 12.57, P <0.001; time F (6, 56) = 35.97, P <0.0001. PWL (**C**): group × time F (6, 48) = 40.23, P <0.0001; group F (1, 8) = 109.2, P < 0.0001; time F (6, 48) = 169.9, P < 0.0001., n = 5 rats per group. (**D**) Representative images showing c-Fos expression in the M1 region. Scale bars: 200μm (low magnification), 50μm (high magnification). (**E** and **F**) Number of c-Fos$^+$ neurons in the M1 region. Sham vs. MIA (**E**): t =2.500, P > 0.05; MIA+tDCS vs. MIA+StDCS (**F**): t =8.050, P < 0.01. n = 5 rats per group. (**G**) Representative images showing c-Fos expression in the PAG. Scale bar: 100μm. (**H**–**J**) Number of c-Fos+ neurons in PAG subregions. DLPAG (**H**): t =0.5164, P > 0.05, LPAG (**I**): t =1.131, P > 0.05, and VLPAG (**J**): t =9.055, P <0.0001. n = 5 rats per group. All data are expressed as mean ± SD. **P < 0.01, ***P < 0.001, ****P < 0.0001; ns indicates not significant.

M1-Targeted tDCS Activates M1 Meanwhile Suppresses vlPAG Hyperactivity in KOA Model Rats

Although MIA alone did not activate M1 neurons (Figure 3D and E; unpaired t-test, Sham vs. MIA: P > 0.05), tDCS stimulation consistently increased activity of M1 neurons. In detail, MIA+tDCS group exhibited a significant increase in M1 c-Fos-positive neurons compared to the MIA+StDCS group (Figure 3D and F; unpaired t-test, MIA+tDCS vs. MIA +StDCS: P < 0.01), supporting the notion that the analgesic effect of tDCS may associated with M1 activation. Additionally, we observed that M1-targeted tDCS significantly reduce activity of vlPAG neurons but not DLPAG or LPAG neurons (Figure 3G–J; unpaired t-test, MIA+tDCS vs. MIA+StDCS, vlPAG: P <0.0001; dlPAG: P > 0.05; lPAG: P > 0.05). These findings suggest that M1 tDCS may exert its analgesic effect, at least partially via suppressing MIA-induced hyperactivity of vlPAG neurons.

M1-Targeted tDCS Rescues Abnormal Activation of vlPAG Microglial in KOA Model Rats

We further evaluated the effect of M1-targeted tDCS on microglial morphology and inflammatory factors expression in the vlPAG of KOA model rats. Immunofluorescence combined with Sholl analysis revealed that microglial in the MIA +tDCS group displayed features of a resting state (Figure 4A): increased branching complexity (Figure 4B; Two-way repeated measure ANOVA and Sidak's multiple comparisons test, MIA+tDCS vs. MIA+StDCS, $P < 0.0001$ at 13–37μm), more distal branches and terminal points, longer maximum branch length, reduced soma size, and decreased Iba-1-positive cells compared with the MIA+StDCS group (Figure 4C–G; unpaired *t*-test, MIA+tDCS vs. MIA+StDCS, $P < 0.05$ to $P < 0.0001$). These morphological changes indicate that tDCS markedly suppresses pro-inflammatory activation of vlPAG microglial. Our qPCR results further demonstrated that tDCS significantly downregulated pro-inflammatory cytokines (IL-6, IL-1β, TNF-α) and upregulated anti-inflammatory cytokines (IL-4 and IL-10) in the vlPAG (Figure 4H–L; unpaired *t*-test, MIA+tDCS vs. MIA+StDCS, $P < 0.05$ to $P < 0.0001$), suggesting that tDCS effectively alleviates microglial activation and neuroinflammation.

The M1 Region Projects Directly to the vlPAG Region via Neural Fibers

Although previous studies have shown that electrical stimulation of M1 produces significant analgesic effects,[32,50] the circuit mechanisms remain unclear. To check whether there were direct projections from M1 to the vlPAG, we injected the retrograde tracer CTB-555 into the vlPAG. Fluorescence-labeled neurons were observed in M1 following CTB-555 injection into the vlPAG (Figure 4M). This anatomical evidence supports the hypothesis that M1 stimulation may induce analgesia by directly modulating vlPAG neuronal activity and engaging descending pain pathways.

Discussion

Pain associated with KOA is characteristically chronic and persistent, with central sensitization serving as a key underlying mechanism.[51] Compared with other osteoarthritis (OA) models, the MIA model more effectively disrupts cartilage and replicates end-stage OA pathology.[52] Previous work has shown that intra-articular injection of high-dose MIA induces robust pain hypersensitivity and central sensitization.[41] In the present study, both PWT and PWL decreased progressively following MIA injection and reached their lowest values on day 14, consistent with sustained pain hypersensitivity. These results are in line with previous reports.[34,35,41] Therefore, day 14 after MIA injection was selected as the time point indicating successful KOA model establishment.

Recent studies have identified the PAG as a central hub in chronic pain regulation, integrating ascending nociceptive input and descending modulatory signals.[53,54] The vlPAG, in particular, plays a critical role in chronic neuropathic pain.[29] In this study, we observed a significant increase in c-Fos-positive neurons in the vlPAG of MIA-induced KOA model rats, indicating neuronal activation in this area during chronic KOA pain. In contrast, other PAG subregions showed less pronounced activation, suggesting that they may be more likely involved in regulating emotion, anxiety, or avoidance behaviors.[55] Our data thus support the idea that the vlPAG is a key brain region in the central regulation of KOA-related chronic pain.

Microglial, as resident immune cells of the CNS, are essential for the development and maintenance of chronic pain and central sensitization.[56] Previous studies have reported significant microglial activation in the anterior cingulate cortex in chronic arthritic hyperalgesia and in the vlPAG in neuropathic pain models.[29,57] Because of the close interaction between neurons and microglial, neuronal hyperactivity can trigger microglial activation, which in turn releases pro-inflammatory cytokines that exacerbate central sensitization.[58] In our MIA-induced KOA pain model, we observed a typical pro-inflammatory activation state of vlPAG microglial. These inflammatory mediators, such as IL-6, IL-1β, and TNF-α, may enhance neuronal excitability and amplify pain signaling by acting on neuronal receptors (eg., IL-1R1, TNF-R) and downstream signaling pathways (eg., NF-κB, MAPK), thereby inducing immediate-early genes expression, such as c-Fos.[59]

Minocycline, a microglial inhibitor, has been shown to effectively alleviate chronic pain in various models.[60] In this study, pre-microinjection of minocycline into the vlPAG significantly prevent microglial activation, reduced neuronal activity and c-Fos expression, and improved PWT and PWL, thereby exerting robust analgesic effects. These findings

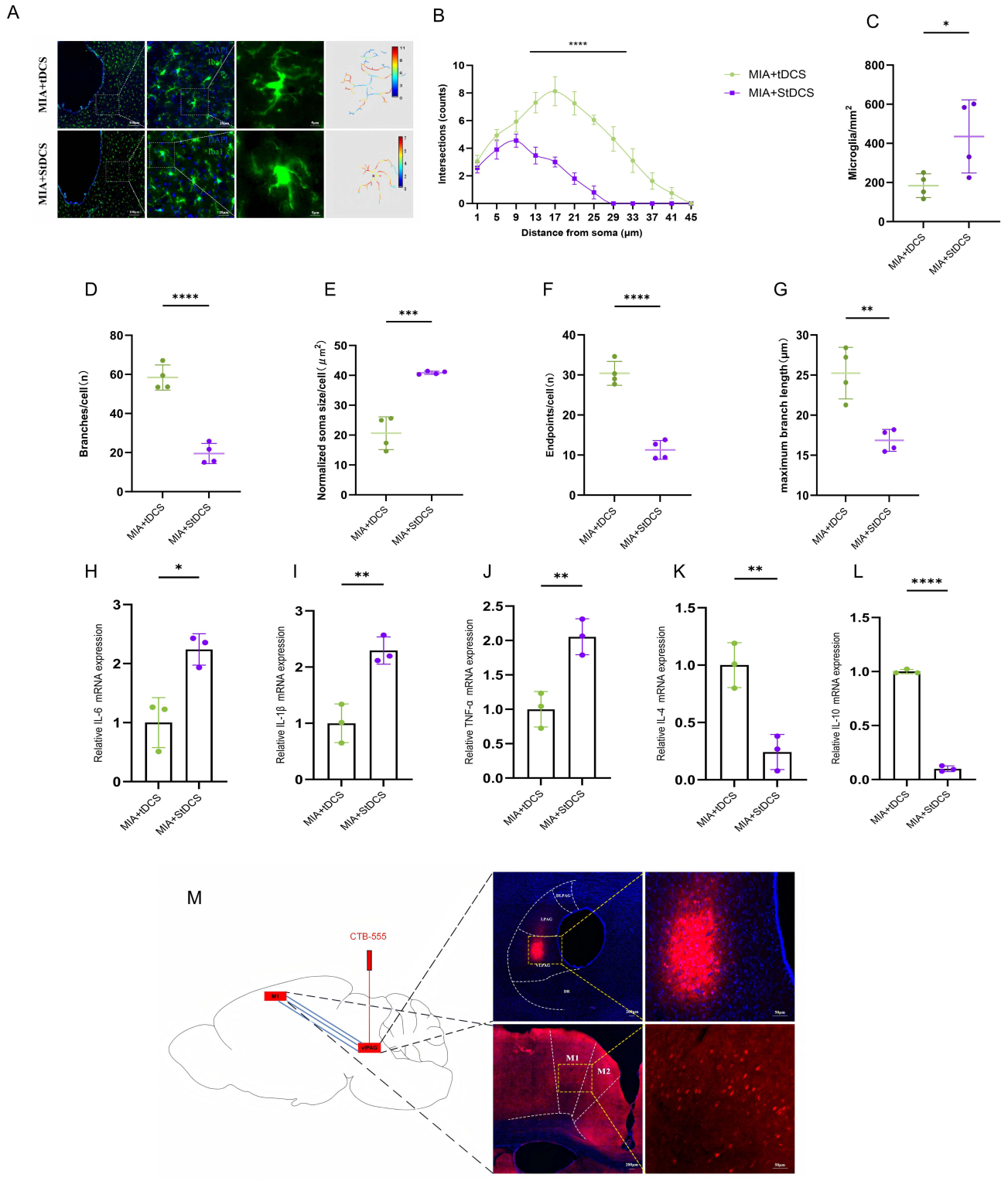

Figure 4 M1-targeted tDCS treatment significantly suppresses microglial activation and pro-inflammatory cytokine release in the vlPAG of MIA-induced KOA rats, possibly mediated by direct neural fiber projections. (**A**) Representative images showing Iba-1$^+$ microglial in vlPAG and the corresponding heatmap. Scale bars: 100μm (left), 20μm (middle), 5μm (right). (**B**) Sholl analysis about intersections with concentric circles. Group × distance from soma F (11, 72) = 28.21, P <0.0001; group F (1, 72) = 587.1, P <0.0001; distance from soma F (11, 72) = 108.0, P <0.0001. n = 3 rats per group. (**C**–**G**) Microglial number and morphology analysis. Microglial counts/mm^2 (**C**): t =2.562, P <0.05; branches/cell (**D**): t =9.435, P <0.0001; soma size/cell (**E**): t =7.345, P <0.001; terminal endpoints (**F**): t =10.09, P <0.0001;maximum process length (**G**): t =4.806, P < 0.01. n = 4 rats per group. (**H**–**L**) RT-qPCR analyses for inflammatory factors expression in the vlPAG. IL-6 (**H**): t =4.294, P <0.05; IL-1β(**I**): t =5.327, P <0.01;TNF-α(**J**): t =4.975, P< 0.01;IL-4 (**K**): t =5.278, P < 0.01; IL-10 (**L**): t =47.10, P <0.0001. n = 3 rats per group. (**M**) A direct projection from M1 to vlPAG revealed by retrograde tracing. An retrograde tracer CTB-555 was microinjected into the vlPAG. Two weeks later CTB-555-labeled neurons (red) were observed in the M1 cortex. Scale bars: 200 μm (low magnification), 50 μm (high magnification). All data are expressed as mean ± SD. *P < 0.05, **P < 0.01, ***P < 0.001, ****P < 0.0001.

https://doi.org/10.2147/JPR.S595212

further support the concept that microglial activation in the vlPAG is a key pathophysiological mechanism in KOA-associated chronic pain, and that microglial-neuron interactions critically shape neuronal activity in this region.

In recent years, tDCS has gained increasing attention as a non-invasive neuromodulation approach for chronic pain management. Studies have shown that tDCS can alleviate various pain conditions, including fibromyalgia and neuropathic pain, by activating endogenous opioid and noradrenergic systems, and modulating neuronal membrane potentials.[61,62] Our previous studies demonstrated that M1-targeted tDCS exerts significant analgesic effects in KOA model rats.[34,35] The present study further shows that the analgesic effect of M1 tDCS persists for at least 7 days, indicating sustained efficacy. However, the mechanism by which weak cortical stimulation influences remote structures such as the PAG remains incompletely understood.[63,64] Using CTB-555 retrograde tracing, we identified direct neural projections from Layer V neurons in M1 to the vlPAG, providing an anatomical substrate for tDCS-mediated modulation of vlPAG function. This finding is consistent with recent reports and suggests that tDCS may regulate vlPAG activity through the M1-vlPAG direct pathway.[65]

In MIA-induced KOA pain model rats, c-Fos expression in M1 region did not differ significantly from that in sham animals, suggesting that M1 itself does not directly participate in KOA pain signaling. Clinical studies have also reported that motor cortex excitability in KOA patients does not differ markedly from healthy controls, potentially reflecting reduced movement and suppressed motor cortex activation associated with chronic pain.[66] Following tDCS, however, M1 exhibited marked activation, accompanied by reduced vlPAG neuronal activity and suppressed microglial activation, indicating functional coupling between these regions. Given the heterogeneity of vlPAG neuronal population, this effect may involve specific neuron subtypes or local interneurons.[67]

Based on our findings, we propose that M1-targeted tDCS exerts its analgesic effects, at least partially, by modulating neuronal and microglial activity in the vlPAG via a direct M1-vlPAG pathway. tDCS significantly suppresses microglial activation, reduces pro-inflammatory cytokine expression, and attenuates neuronal hyperactivity, highlighting this "cortex-midbrain" regulatory pathway as a promising target for chronic pain management.

Our present study has several limitations. First, some experiments were conducted with relatively small sample sizes, which may increase the risk of type II error and limit the generalizability of the findings. To enhance statistical rigor, post hoc power analyses were performed for experiments with small sample sizes using G*Power 3.1.9.7, and the results are provided in Supplementary Table 1. Accordingly, the present findings should be considered supportive rather than definitive and require further validation in larger, independent cohorts. Second, tDCS was administered under brief isoflurane anesthesia. Although this approach ensured stable electrode placement and minimized stress-related movement, isoflurane itself may influence pain-related behaviors, neuronal excitability, and neuroinflammatory responses, including microglial activation.[68] In addition, a dedicated sham-anesthesia control group was not included. Future studies employing awake stimulation paradigms or incorporating additional sham-anesthesia controls are warranted to better isolate the specific effects of tDCS from those of anesthetic exposure. Third, this study exclusively used male rats. While this approach reduced biological variability, it limits the generalizability of the findings. Accumulating evidence indicates that pain processing and microglial-mediated hypersensitivity are highly sex-dependent, often exhibiting greater microglial involvement in males than in females.[69,70] Consequently, the effects of tDCS and minocycline on vlPAG microglial observed in this study may differ in females. Therefore, caution is required when extrapolating these findings to clinical populations, and future studies including female animals are necessary to clarify sex-specific mechanisms and improve translational relevance. Fourth, a dedicated vehicle or site-specific control was not included. As a result, non-specific behavioral effects related to local infusion or tissue disturbance cannot be completely excluded. Although a small injection volume and slow infusion rate were used to minimize these effects, future studies incorporating vehicle controls and adjacent-site injections will be necessary to more rigorously confirm the anatomical and pharmacological specificity of the observed effects. Fifth, the MIA-induced KOA model is chemically driven and does not fully recapitulate the gradual progression of human degenerative OA. While this limits direct clinical translation, the model remains a well-established and widely accepted tool for investigating pain mechanisms and evaluating potential therapeutic strategies.

Conclusion

In summary, this study demonstrates that M1-targeted tDCS alleviates chronic pain-related behaviors in a rat model of KOA, at least in part, by modulating neuronal activity and microglial-mediated neuroinflammation within the vlPAG. Modulation of the direct M1-vlPAG pathway may underlie the observed analgesic effects. These findings provide novel preclinical evidence supporting the potential of non-invasive brain stimulation for the treatment of chronic pain. Although the results may have translational relevance, their implications for human pain management remain preliminary and require further clinical validation. Future studies should focus on elucidating the precise cellular and circuit-level mechanisms involved and identifying specific therapeutic targets within this pathway to enable the development of more targeted and effective interventions for chronic pain disorders, including KOA.

Description of Euthanasia and Anesthesia Methods

1. Pre-anesthesia preparation: Conduct a comprehensive physical examination of SD rats preoperatively. Based on their body weight (typically 200–300g), accurately calculate the dosages of various medications. Withhold food for 4–6 hours and water for 2–3 hours (to prevent vomiting and aspiration during anesthesia). Ensure the operating environment is sterile and maintains an appropriate temperature (23–25°C), avoiding environmental stressors that may cause distress to the rats.
2. The anesthesia was administered via intraperitoneal injection using sodium pentobarbital (manufactured by Beijing Ludun Biotechnology Co., Ltd). The dosage was calculated at 50 mg/kg based on the body weight of the SD rats. The solution was slowly injected intraperitoneally until the rats exhibited the disappearance of the eyelid reflex, muscle relaxation, and stable respiration (respiratory rate maintained at 50–80 breaths per minute), indicating entry into an anesthetized state, at which point the injection was stopped. Respiratory and heart rate changes were monitored throughout the procedure.
3. Euthanasia was performed via intraperitoneal injection using sodium pentobarbital at a dosage approximately three times the anesthetic dose, calculated as roughly 100–150 mg/kg based on the body weight of the SD rats. The solution was administered slowly via intravenous push while closely monitoring the rat's response, until cessation of both heart rate and respiration was observed.
4. Anesthesia was maintained via inhalation using isoflurane (specification: 100 mL/bottle; manufacturer: RWD), which was administered through a miniature anesthesia machine. The inhalation concentration was maintained at 1.5%–2.0%. Vital signs were monitored continuously throughout the procedure, with heart rate, respiration, blood oxygen saturation, and body temperature (normal range for SD rats: 36.5–38.5°C) recorded every 3 minutes.[71,72]
5. Compliance Basis: The entire systemic anesthesia procedure for the SD rats strictly adhered to the American Veterinary Medical Association (AVMA) Guidelines for Animal Anesthesia (latest edition) and the Standard Protocol for Rodent Experimental Anesthesia. The selection of anesthetic agents, dosage calculations, and operational procedures (such as tail vein injection and the use of miniature anesthesia equipment) all complied with the relevant specifications for systemic anesthesia in SD rats outlined in these guidelines. This ensured the safety and efficacy of anesthesia while minimizing stress and discomfort for the rats.

Data Sharing Statement

The raw behavioral data, original immunofluorescence images, Sholl analysis source images, and qPCR Ct values generated in this study are available from the corresponding author upon reasonable request.

Ethics Approval and Consent to Participate

All experimental protocols were approved by the Animal Care and Use Committee of Qingdao University (approval number: 20240710SD6420240821092) and were carried out in accordance with the guidelines of the International Association for the Study of Pain. Moreover, the study is reported in accordance with ARRIVE guidelines.

Acknowledgments

The authors wish to acknowledge the Physiology Laboratory of Qingdao University for providing the experimental site and equipment for our study.

Author Contributions

TL and YZ designed the study. YX conducted the research. CF acquired the data, JX interpreted the data, and CG analyzed the data. All authors made a significant contribution to the work reported, whether that is in the conception, study design, execution, acquisition of data, analysis and interpretation, or in all these areas; took part in drafting, revising or critically reviewing the article; gave final approval of the version to be published; have agreed on the journal to which the article has been submitted; and agree to be accountable for all aspects of the work.

Funding

This work was supported by the Natural Science Foundation of Shandong Province (Grant No. RZ2300003797).

Disclosure

The authors declare no competing interests in this work.

References

1. Thakur M, Rahman W, Hobbs C, Dickenson AH, Bennett DLH, Baccei ML. Characterisation of a peripheral neuropathic component of the rat monoiodoacetate model of osteoarthritis. *PLoS One*. 2012;7(3):e33730. doi:10.1371/journal.pone.0033730
2. Miller RE, Malfait AM. Osteoarthritis pain: what are we learning from animal models? *Best Pract Res Clin Rheumatol*. 2017;31(5):676–687. doi:10.1016/j.berh.2018.03.003
3. Bannuru RR, Osani MC, Vaysbrot EE, et al. OARSI guidelines for the non-surgical management of knee, Hip, and polyarticular osteoarthritis. *Osteoarthritis Cartilage*. 2019;27(11):1578–1589. doi:10.1016/j.joca.2019.06.011
4. Kolasinski SL, Neogi T, Hochberg MC, et al. 2019 American College of Rheumatology/Arthritis Foundation Guideline for the Management of Osteoarthritis of the Hand, Hip, and Knee. *Arthritis Care Res*. 2020;72(2):149–162. doi:10.1002/acr.24131
5. Hochberg MC, Altman RD, April KT, et al. American College of Rheumatology 2012 recommendations for the use of nonpharmacologic and pharmacologic therapies in osteoarthritis of the hand, Hip, and knee. *Arthritis Care Res*. 2012;64(4):465–474. doi:10.1002/acr.21596
6. Bourne RB, Chesworth BM, Davis AM, Mahomed NN, Charron KD. Patient satisfaction after total knee arthroplasty: who is satisfied and who is not? *Clin Orthop Relat Res*. 2010;468(1):57–63. doi:10.1007/s11999-009-1119-9
7. Velly AM, Look JO, Carlson C, et al. The effect of catastrophizing and depression on chronic pain--a prospective cohort study of temporomandibular muscle and joint pain disorders. *Pain*. 2011;152(10):2377–2383. doi:10.1016/j.pain.2011.07.004
8. Lluch Girbés E, Nijs J, Torres-Cueco R, López Cubas C. Pain treatment for patients with osteoarthritis and central sensitization. *Phys Ther*. 2013;93(6):842–851. doi:10.2522/ptj.20120253
9. Eckstein F, Cotofana S, Wirth W, et al. Greater rates of cartilage loss in painful knees than in pain-free knees after adjustment for radiographic disease stage: data from the osteoarthritis initiative. *Arthritis Rheum*. 2011;63(8):2257–2267. doi:10.1002/art.30414
10. Volcheck MM, Graham SM, Fleming KC, Mohabbat AB, Luedtke CA. Central sensitization, chronic pain, and other symptoms: better understanding, better management. *Cleve Clin J Med*. 2023;90(4):245–254. doi:10.3949/ccjm.90a.22019
11. Ji -R-R, Nackley A, Huh Y, Terrando N, Maixner W. Neuroinflammation and Central Sensitization in Chronic and Widespread Pain. *Anesthesiology*. 2018;129(2):343–366. doi:10.1097/aln.0000000000002130
12. Mantyh PW. Connections of midbrain periaqueductal gray in the monkey. II. Descending efferent projections. *J Neurophysiol*. 1983;49(3):582–594. doi:10.1152/jn.1983.49.3.582
13. Yin J-B, Wu -H-H, Dong Y-L, et al. Neurochemical properties of BDNF-containing neurons projecting to rostral ventromedial medulla in the ventrolateral periaqueductal gray. *Front Neural Circuits*. 2014;8:137. doi:10.3389/fncir.2014.00137
14. Xie L, Wu H, Chen Q, et al. Divergent modulation of pain and anxiety by GABAergic neurons in the ventrolateral periaqueductal gray and dorsal raphe. *Neuropsychopharmacology*. 2023;48(10):1509–1519. doi:10.1038/s41386-022-01520-0
15. Zhu X, Zhang C, Hu Y, et al. Modulation of Comorbid Chronic Neuropathic Pain and Anxiety-Like Behaviors by Glutamatergic Neurons in the Ventrolateral Periaqueductal Gray and the Analgesic and Anxiolytic Effects of Electroacupuncture. *eNeuro*. 2024;11(8):2. doi:10.1523/eneuro.0454-23.2024
16. Wang J, Zhang H, Feng YP, et al. Morphological evidence for a neurotensinergic periaqueductal gray-rostral ventromedial medulla-spinal dorsal horn descending pathway in rat. *Front Neuroanat*. 2014;8:112. doi:10.3389/fnana.2014.00112
17. Gao T, Wang C, Yang X, He Z, Wang Y, Mi W. Hyperoside ameliorates neuropathic pain by modulating the astroglial reactivity in the vlPAG. *Neuropharmacology*. 2025;266:110276. doi:10.1016/j.neuropharm.2024.110276
18. Linnman C, Moulton EA, Barmettler G, Becerra L, Borsook D. Neuroimaging of the periaqueductal gray: state of the field. *Neuroimage*. 2012;60(1):505–522. doi:10.1016/j.neuroimage.2011.11.095
19. Mills EP, Di Pietro F, Alshelh Z, et al. Brainstem Pain-Control Circuitry Connectivity in Chronic Neuropathic Pain. *J Neurosci*. 2018;38(2):465–473. doi:10.1523/jneurosci.1647-17.2017

20. Fregni F, El-Hagrassy MM, Pacheco-Barrios K, et al. Evidence-Based Guidelines and Secondary Meta-Analysis for the Use of Transcranial Direct Current Stimulation in Neurological and Psychiatric Disorders. *Int J Neuropsychopharmacol*. 2021;24(4):256–313. doi:10.1093/ijnp/pyaa051
21. Hu X, Du L, Liu S, et al. A TRPV4-dependent neuroimmune axis in the spinal cord promotes neuropathic pain. *J Clin Invest*. 2023;133(5):3. doi:10.1172/jci161507
22. Haidar MA, Ibeh S, Shakkour Z, et al. Crosstalk between microglial and Neurons in Neurotrauma: an Overview of the Underlying Mechanisms. *Curr Neuropharmacol*. 2022;20(11):2050–2065. doi:10.2174/1570159x19666211202123322
23. Brown EV, Falnikar A, Heinsinger N, et al. Cervical spinal cord injury-induced neuropathic pain in male mice is associated with a persistent pro-inflammatory macrophage/microglial response in the superficial dorsal horn. *Exp Neurol*. 2021;343:113757. doi:10.1016/j.expneurol.2021.113757
24. Nakamura Y, Fukuta A, Miyashita K, et al. Perineural high-mobility group box 1 induces mechanical hypersensitivity through activation of spinal microglial: involvement of glutamate-NMDA receptor dependent mechanism in spinal dorsal horn. *Biochem Pharmacol*. 2021;186:114496. doi:10.1016/j.bcp.2021.114496
25. Crain JM, Nikodemova M, Watters JJ. Expression of P2 nucleotide receptors varies with age and sex in murine brain microglial. *J Neuroinflammation*. 2009;6:24. doi:10.1186/1742-2094-6-24
26. Ho YH, Lin YT, Wu CW, Chao YM, Chang AY, Chan JY. Peripheral inflammation increases seizure susceptibility via the induction of neuroinflammation and oxidative stress in the hippocampus. *J Biomed Sci*. 2015;22(1):46. doi:10.1186/s12929-015-0157-8
27. Nieto FR, Clark AK, Grist J, Hathway GJ, Chapman V, Malcangio M. Neuron-immune mechanisms contribute to pain in early stages of arthritis. *J Neuroinflammation*. 2016;13(1):96. doi:10.1186/s12974-016-0556-0
28. Fernandez-Zafra T, Gao T, Jurczak A, et al. Exploring the transcriptome of resident spinal microglial after collagen antibody-induced arthritis. *Pain*. 2019;160(1):224–236. doi:10.1097/j.pain.0000000000001394
29. Ni HD, Yao M, Huang B, et al. Glial activation in the periaqueductal gray promotes descending facilitation of neuropathic pain through the p38 MAPK signaling pathway. *J Neurosci Res*. 2016;94(1):50–61. doi:10.1002/jnr.23672
30. Fregni F, Freedman S, Pascual-Leone A. Recent advances in the treatment of chronic pain with non-invasive brain stimulation techniques. *Lancet Neurol*. 2007;6(2):188–191. doi:10.1016/s1474-4422(07)70032-7
31. Benninger DH, Lomarev M, Lopez G, et al. Transcranial direct current stimulation for the treatment of Parkinson's disease. *J Neurol Neurosurg Psychiatry*. 2010;81(10):1105–1111. doi:10.1136/jnnp.2009.202556
32. Alappat JJ. Motor cortex stimulation for chronic pain: systematic review and meta-analysis of the literature. *Neurology*. 2009;72(6):577. doi:10.1212/01.wnl.0000344169.51931.e5
33. Tan M, Feng Z, Chen H, et al. Transcranial direct current stimulation regulates phenotypic transformation of microglial to relieve neuropathic pain induced by spinal cord injury. *Front Behav Neurosci*. 2023;17:1147693. doi:10.3389/fnbeh.2023.1147693
34. Ye Y, Yan X, Wang L, Xu J, Li T. Transcranial direct current stimulation attenuates chronic pain in knee osteoarthritis by modulating BDNF/TrkB signaling in the descending pain modulation system. *Neurosci Lett*. 2023;810:137320. doi:10.1016/j.neulet.2023.137320
35. Li X, Zhou W, Wang L, Ye Y, Li T. Transcranial Direct Current Stimulation Alleviates the Chronic Pain of Osteoarthritis by Modulating NMDA Receptors in Midbrain Periaqueductal Gray in Rats. *J Pain Res*. 2022;15:203–214. doi:10.2147/jpr.S333454
36. Ahn H, Woods AJ, Kunik ME, et al. Efficacy of transcranial direct current stimulation over primary motor cortex (anode) and contralateral supraorbital area (cathode) on clinical pain severity and mobility performance in persons with knee osteoarthritis: an experimenter- and participant-blinded, randomized, sham-controlled pilot clinical study. *Brain Stimul*. 2017;10(5):902–909. doi:10.1016/j.brs.2017.05.007
37. García-Larrea L, Peyron R, Mertens P, et al. Electrical stimulation of motor cortex for pain control: a combined PET-scan and electrophysiological study. *Pain*. 1999;83(2):259–273. doi:10.1016/s0304-3959(99)00114-1
38. Brunoni AR, Nitsche MA, Bolognini N, et al. Clinical research with transcranial direct current stimulation (tDCS): challenges and future directions. *Brain Stimul*. 2012;5(3):175–195. doi:10.1016/j.brs.2011.03.002
39. Lefaucheur JP, Antal A, Ayache SS, et al. Evidence-based guidelines on the therapeutic use of transcranial direct current stimulation (tDCS). *Clin Neurophysiol*. 2017;128(1):56–92. doi:10.1016/j.clinph.2016.10.087
40. Eitner A, Hofmann GO, Schaible HG. Mechanisms of Osteoarthritic Pain. Studies in Humans and Experimental Models. *Front Mol Neurosci*. 2017;10:349. doi:10.3389/fnmol.2017.00349
41. Havelin J, Imbert I, Cormier J, Allen J, Porreca F, King T. Central Sensitization and Neuropathic Features of Ongoing Pain in a Rat Model of Advanced Osteoarthritis. *J Pain*. 2016;17(3):374–382. doi:10.1016/j.jpain.2015.12.001
42. Luppi PH, Fort P, Jouvet M. Iontophoretic application of unconjugated cholera toxin B subunit (CTb) combined with immunohistochemistry of neurochemical substances: a method for transmitter identification of retrogradely labeled neurons. *Brain Res*. 1990;534(1–2):209–224. doi:10.1016/0006-8993(90)90131-t
43. Liu R, Zhu T, Chu X, et al. Transcranial direct current stimulation alleviates chronic pain in knee osteoarthritis by modulating microglial and astrocytic polarization and neuroinflammation. *Life Sci*. 2025;376:123753. doi:10.1016/j.lfs.2025.123753
44. Chaplan SR, Bach FW, Pogrel JW, Chung JM, Yaksh TL. Quantitative assessment of tactile allodynia in the rat paw. *J Neurosci Methods*. 1994;53(1):55–63. doi:10.1016/0165-0270(94)90144-9
45. Hargreaves K, Dubner R, Brown F, Flores C, Joris J. A new and sensitive method for measuring thermal nociception in cutaneous hyperalgesia. *Pain*. 1988;32(1):77–88. doi:10.1016/0304-3959(88)90026-7
46. Spezia Adachi LN, Quevedo AS, de Souza A, et al. Exogenously induced brain activation regulates neuronal activity by top-down modulation: conceptualized model for electrical brain stimulation. *Exp Brain Res*. 2015;233(5):1377–1389. doi:10.1007/s00221-015-4212-1
47. Lopes BC, Medeiros LF, Silva de Souza V, et al. Transcranial direct current stimulation combined with exercise modulates the inflammatory profile and hyperalgesic response in rats subjected to a neuropathic pain model: long-term effects. *Brain Stimul*. 2020;13(3):774–782. doi:10.1016/j.brs.2020.02.025
48. Johnson GA, Calabrese E, Badea A, Paxinos G, Watson C. A multidimensional magnetic resonance histology atlas of the Wistar rat brain. *Neuroimage*. 2012;62(3):1848–1856. doi:10.1016/j.neuroimage.2012.05.041
49. Liu Q, Tang S, Du X, Sun Y, Lai J, Wang X. Injection of minocycline into the periaqueductal gray attenuates morphine withdrawal signs. *Neurosci Lett*. 2020;736:135283. doi:10.1016/j.neulet.2020.135283
50. Knotkova H, Hamani C, Sivanesan E, et al. Neuromodulation for chronic pain. *Lancet*. 2021;397(10289):2111–2124. doi:10.1016/s0140-6736(21)00794-7
51. Mansfield CJ, Culiver A, Briggs M, Schmitt LC, Grooms DR, Oñate J. The effects of knee osteoarthritis on neural activity during a motor task: a scoping systematic review. *Gait Posture*. 2022;96:221–235. doi:10.1016/j.gaitpost.2022.05.035

52. Kuyinu EL, Narayanan G, Nair LS, Laurencin CT. Animal models of osteoarthritis: classification, update, and measurement of outcomes. *J Orthop Surg Res*. 2016;11:19. doi:10.1186/s13018-016-0346-5
53. Bandler R, Shipley MT. Columnar organization in the midbrain periaqueductal gray: modules for emotional expression? *Trends Neurosci*. 1994;17 (9):379–389. doi:10.1016/0166-2236(94)90047-7
54. Noh ASM, Ismail CAN. A Review on Chronic Pain in Rheumatoid Arthritis: a Focus on Activation of NR2B Subunit of N-Methyl-D-Aspartate Receptors. *Malays J Med Sci*. 2020;27(1):6–21. doi:10.21315/mjms2020.27.1.2
55. Graeff FG, Sant'Ana AB, Vilela-Costa HH, Zangrossi Jr H. New Findings on the Neurotransmitter Modulation of Defense in the Dorsal Periaqueductal Gray. *CNS Neurol Disord Drug Targets*. 2015;14(8):988–995. doi:10.2174/1871527314666150909114558
56. Zhang WJ, Luo HL, Zhu ZM. The role of P2X4 receptors in chronic pain: a potential pharmacological target. *Biomed Pharmacother*. 2020;129:110447. doi:10.1016/j.biopha.2020.110447
57. Pan TT, Gao W, Song ZH, et al. Glutamatergic neurons and myeloid cells in the anterior cingulate cortex mediate secondary hyperalgesia in chronic joint inflammatory pain. *Brain Behav Immun*. 2022;101:62–77. doi:10.1016/j.bbi.2021.12.021
58. Marinelli S, Basilico B, Marrone MC. Ragozzino D. microglial-neuron crosstalk: signaling mechanism and control of synaptic transmission. *Semin Cell Dev Biol*. 2019;94:138–151. doi:10.1016/j.semcdb.2019.05.017
59. Tsuda M, Shigemoto-Mogami Y, Koizumi S, et al. P2X4 receptors induced in spinal microglial gate tactile allodynia after nerve injury. *Nature*. 2003;424(6950):778–783. doi:10.1038/nature01786
60. Zhou YQ, Liu DQ, Chen SP, et al. Minocycline as a promising therapeutic strategy for chronic pain. *Pharmacol Res*. 2018;134:305–310. doi:10.1016/j.phrs.2018.07.002
61. Moshfeghinia R, Shekouh D, Mostafavi S, et al. The effects of transcranial direct-current stimulation (tDCS) on pain intensity of patients with fibromyalgia: a systematic review and meta-analysis. *BMC Neurol*. 2023;23(1):395. doi:10.1186/s12883-023-03445-7
62. Souza A, Martins DF, Medeiros LF, et al. Neurobiological mechanisms of antiallodynic effect of transcranial direct current stimulation (tDCS) in a mice model of neuropathic pain. *Brain Res*. 2018;1682:14–23. doi:10.1016/j.brainres.2017.12.005
63. Lima MC, Fregni F. Motor cortex stimulation for chronic pain: systematic review and meta-analysis of the literature. *Neurology*. 2008;70 (24):2329–2337. doi:10.1212/01.wnl.0000314649.38527.93
64. Cioato SG, Medeiros LF, Marques Filho PR, et al. Long-Lasting Effect of Transcranial Direct Current Stimulation in the Reversal of Hyperalgesia and Cytokine Alterations Induced by the Neuropathic Pain Model. *Brain Stimul*. 2016;9(2):209–217. doi:10.1016/j.brs.2015.12.001
65. Gan Z, Gangadharan V, Liu S, et al. Layer-specific pain relief pathways originating from primary motor cortex. *Science*. 2022;378 (6626):1336–1343. doi:10.1126/science.add4391
66. Kittelson AJ, Thomas AC, Kluger BM, Stevens-Lapsley JE. Corticospinal and intracortical excitability of the quadriceps in patients with knee osteoarthritis. *Exp Brain Res*. 2014;232(12):3991–3999. doi:10.1007/s00221-014-4079-6
67. Wan XD, Cai GH, Yan ZQ, et al. PV and SST neurons in the anterior cingulate cortex regulate social disorders in adulthood induced by sensory abnormalities in childhood. *CNS Neurosci Ther*. 2024;30(7):e14863. doi:10.1111/cns.14863
68. Skvarc DR, Berk M, Byrne LK, et al. Post-Operative Cognitive Dysfunction: an exploration of the inflammatory hypothesis and novel therapies. *Neurosci Biobehav Rev*. 2018;84:116–133. doi:10.1016/j.neubiorev.2017.11.011
69. Mogil JS. Qualitative sex differences in pain processing: emerging evidence of a biased literature. *Nat Rev Neurosci*. 2020;21(7):353–365. doi:10.1038/s41583-020-0310-6
70. Sorge RE, Mapplebeck JC, Rosen S, et al. Different immune cells mediate mechanical pain hypersensitivity in male and female mice. *Nat Neurosci*. 2015;18(8):1081–1083. doi:10.1038/nn.4053
71. Gaskill BN, Boykin C, Zuniga I, Maynard K, Scorrano F. Evaluation of Thermal Support during Anesthesia Induction on Body Temperature in C57BL/6 and Nude Mice. *J Am Assoc Lab Anim Sci*. 2024;63(3):294–302. doi:10.30802/aalas-jaalas-23-000085
72. Richardson CA, Flecknell PA. Anaesthesia and post-operative analgesia following experimental surgery in laboratory rodents: are we making progress? *Altern Lab Anim*. 2005;33(2):119–127. doi:10.1177/026119290503300207

Journal of Pain Research

Dovepress
Taylor & Francis Group

Publish your work in this journal

The Journal of Pain Research is an international, peer reviewed, open access, online journal that welcomes laboratory and clinical findings in the fields of pain research and the prevention and management of pain. Original research, reviews, symposium reports, hypothesis formation and commentaries are all considered for publication. The manuscript management system is completely online and includes a very quick and fair peer-review system, which is all easy to use. Visit http://www.dovepress.com/testimonials.php to read real quotes from published authors.

Submit your manuscript here: https://www.dovepress.com/journal-of-pain-research-journal